Research Article

Particle Swarm Optimization for Positioning the Coil of Transcranial Magnetic Stimulation

Congsheng Li, Chang Liu, Lei Yang, Luyang He, and Tongning Wu [ID]

China Academy of Information and Communications Technology, Beijing, China

Correspondence should be addressed to Tongning Wu; toniwoo@gmail.com

The distribution of the induced electric field (E-field) during transcranial magnetic stimulation (TMS) depends on the individual anatomical structure of the brain as well as coil positioning. Inappropriate stimulation may degrade the efficacy of TMS or even induce adverse effects. Therefore, optimizing the E-field according to individual anatomy and clinical need has become a research focus. In this paper, particle swarm optimization (PSO) was applied for the first time to the positioning of TMS coils with anatomical head models. We discuss the parameters of the PSO algorithm, which were optimized to achieve a reasonable convergence time suitable for in-time treatment planning. The optimizer improved the distribution of the induced E-field strength at the dedicated cortical region, with a mean value of 48.31% compared with that from the conventional treatment position. The optimization terminated after 4–11 iterations for 13 head models. The applicability and performance of the optimizer for a large population are discussed in terms of cortical complexity. This study could benefit not only clinics but also research on brain modulation.

1. Introduction

Transcranial magnetic stimulation (TMS) [1] is a widely used, noninvasive tool for modulating brain activity. Short pulses of magnetic fields are delivered to the cortex through current-carrying coils. The rapidly changing magnetic field induces current within the cortex and stimulates activity over a predefined cortical region [2]. Image-based navigation systems could provide accurate and repeatable coil positioning according to anatomical or contour-based landmarks. However, the distribution of the induced electric field (E-field) in the brain depends on individual anatomy [2, 3], such as gyral orientation [4] and the dielectric properties of cortical tissues [2]. The maximum E-field strength is unnecessarily located beneath the focus of the coil, usually by several centimeters [5]. Therefore, the coil's placement and orientation should be optimized to ensure appropriate stimulation of the target region [6–9]. The induced E-field in the target region can be maximized using extensive numerical simulations by traversing all possible configurations. Nevertheless, that process requires a huge time cost, making it unsuitable for in-time clinical planning.

Heuristic algorithms (e.g., genetic algorithm [10, 11] and particle swarm optimization (PSO)) [12] have been reported to facilitate TMS coil design. Inspired by its efficiency at managing convergence rates and search diversity, we applied PSO [12] to the optimization of coil positioning and orientation. Tested using various anatomical head models, the proposed method could enhance local E-field strength by an average value of 48.31% (ranging between 10.98% and 116.57%) compared with the results of stimulation at conventional stimulation position. The number of simulations could be reduced to 3% of that used by the brute force method (traversing all possible configurations). Parametric optimization for PSO has been discussed. The relationship between optimization performance and cortical complexity has been investigated using the local gyrification index (lGI [13]) and local factual dimensionality (lFD [14]). The results have demonstrated the applicability of that method to a large population. The proposed method facilitated individual treatment design with a reasonable time cost. Physicians can

use this method to optimize the E-field distribution before the treatment almost automatically (the time cost can be around 3 to 10 hours as shown in our study by serial computation), without human intervention. Integrated with the navigation system, the proposed method will be beneficial to not only clinics but also brain studies. In addition, it aims to exploit the performance of an existing coil instead of designing a new one, which provides a low-cost option for researchers.

2. Materials and Models

2.1. Numerical Models. Numerical head models from Chinese adult female (23 different tissues) and male (23 different tissues [15, 16]) participants; Billie (24 different tissues), Duke (23 different tissues), and Ella (23 different tissues) from a virtual family [17]; the correspondent author of this study (abbreviated as TWU, 14 different tissues) constructed by aids of the in-house modeling tool [18]; a Japanese male (12 different tissues [19]) participant; a Japanese female (15 different tissues [19]) participant; Norman (8 different tissues [20]); Naomi (8 different tissues [21]); Korean adult (13 different tissues [22]); Korean child (13 different tissues [23]); and VIP-Man (14 different tissues [24]) were used in the simulations (Figures 1(a)–1(m)). All models were remeshed to $1 \times 1 \times 1 \, \text{mm}^3$. A one-turn figure-of-eight (FOE) coil, activated with a time-variant current (1 kA at 2.24 kHz), was used in the simulations (Figure 1(n)). The tissues for the different models and their dielectric properties [25, 26] at the operating frequency (2.24 kHz) are shown in Tables 1 and 2.

2.2. Positioning of the Head/Coil Models in the Simulations. The purpose of optimization was to maximize the E-field strength in the region of interest (ROI) by selecting the position (x, y, z) and rotational angle (φ) of the coil center. The bottom-center of the model was positioned at the origin $(0, 0, 0)$ of the Cartesian coordinate system, while the long axis of the head was aligned to the Z-axis. The coil moved around the scalp with a constant separation of 10 mm (to mimic the space occupied by the protective shell), and its plane was tangential to the surface. The rotational axis passed through the intersection point of the FOE coil and was perpendicular to the coil's surface. A rotational angle of $0°$ was defined as the coil's long axis being parallel to the X coordinate. Clinically, the stimulation was conventionally performed with the ROI beneath the intersection point of the FOE coil. Figures 2(a)–2(c) show the configurations.

2.3. Particle Swarm Optimization. In PSO, a population of candidate particles is moved along the search surface, and measurements are made according to a given measure of quality (mathematical formula) that regulates the particle's solution (representing the coil's position and orientational angle in our study) and velocity [27]. Each particle's movement is influenced by its known position and that of the population in the search space. As such, the swarm is expected to move toward the best solutions.

PSO was initialized with a number of particles to search for optima. The solution of the particle at the ith iteration was

$$\text{pos}_i = (x_i, \, y_i, \, z_i, \, \varphi_i), \tag{1}$$

where x_i, y_i, and z_i represent the coordinates of the position of the coil center at the ith iteration, where φ_i is the coil's orientational angle at the ith iteration.

The particle updates its velocity and position according to

$$v_i = \omega v_i + c_1 \times \text{rand}\,()\left(\text{pos}_{pi} - \text{pos}_i\right) + c_2 \times \text{rand}\,()$$
$$\times \left(\text{pos}_{pg} - \text{pos}_i\right), \tag{2}$$
$$\text{pos}_i = \text{pos}_i + v_i,$$

where rand() is a random number between 0 and 1. c_1 and c_2 are learning factors (exploration and exploitation abilities), and usually, $c_1 = c_2 = 2$ to balance cognitive and social influences. ω is the inertial weight factor, which is between 0.9 and 1.2 [27]. The self-adaptive method is $\omega = \omega_{\max} - t/t_{\max}(\omega_{\max} - \omega_{\min})$ [28], with $\omega_{\min}$ and $\omega_{\max}$ being the minimum and maximum weights, respectively. t and $t_{\max}$ are the current iterative number and the maximum iterative number, respectively. pos_{pi} is the best solution that a particle has ever achieved, and pos_{pg} is the best solution of the particle swarm.

The coil was rotated along the axis (φ) with a step of $15°$. The particles were initiated on a curved surface of $4 \times 4 \, \text{cm}^2$ spread over the cortex (with a spacing of 10 mm), and the ROI was located beneath its center.

The optimization program was coded in Python.

2.4. Numerical Solver and Hardware. The in-house ELF scalar potential finite difference (SPFD) solver was used to calculate the induced E-field distribution in the brains [29]. The solver used the incomplete lower- and upper-matrix preconditioner to speed up solution of the derived septa-diagonal matrix, where block Forward-Elimination and Backward-Substitution algorithms were developed to facilitate GPU-based multithread parallelization. This solver has been validated with commercial software and has been demonstrated to have high computational efficiency when processing ELF MF problems [29]. The solver's code is free to download at https://github.com/licongsheng/OpenSPFD.

The simulation volume was discretized into $1 \times 1 \times 1 \, \text{mm}^3$ voxels. The hardware configuration was as follows: CPU: $2 \times$ Xeon E5-2630, 2.2 GHz; memory on board: 256 GB; GPU: $2 \times$ NVIDIA Tesla K40c with 24 GB total memory. The numerical simulation of each head under TMS with the given configuration took about 6 min.

2.5. Numerical Experiment. In this study, stimulation of the motor cortex was used to evaluate the effects of optimization. The motor cortex is involved in the planning, control, and execution of voluntary movements, and it is one of the most frequently stimulated regions in diagnostic
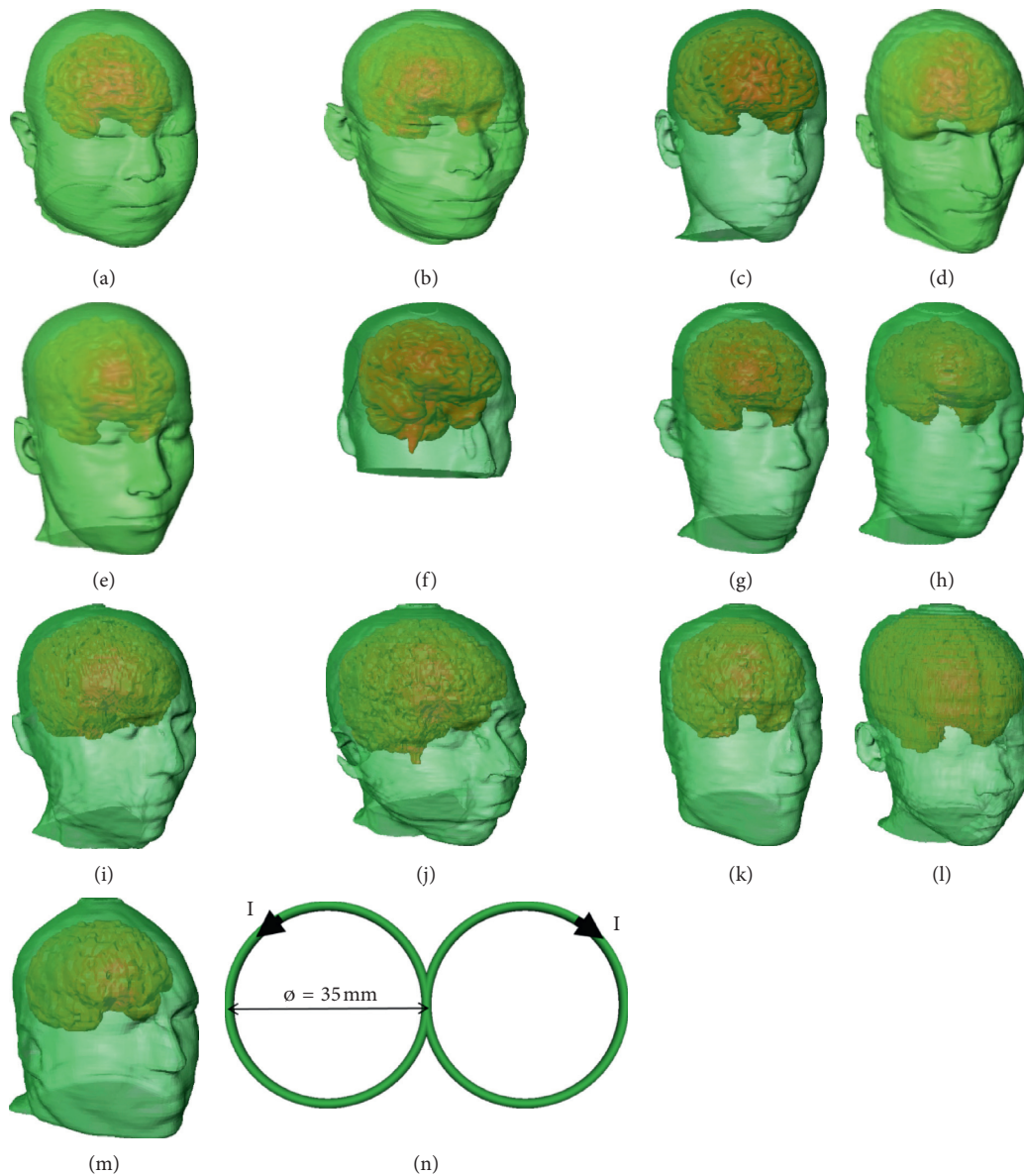
Figure 1: Anatomical head model and the coil model used in the numerical study. The head models are from (a) Chinese female model, (b) Chinese male model, (c) Billie, (d) Duke, (e) Ella, (f) TWU, (g) Japanese male, (h), Japanese female, (i) Norman, (j) Naomi, (k) Korean adult, (l) Korean child, and (m) VIP-Man. (n) The figure-of-eight coil model used in the simulation with I representing current in the coil.

and therapeutic applications [30]. The motor cortex can be divided into the primary motor cortex, premotor cortex, and supplementary motor area, with specific sites corresponding to various body movements [31, 32]. Previous experimental and modeling-based reports have suggested that the size of a given muscle's representation is rather narrow [33]. In this numerical trial, a surface of $2 \times 2 \, \text{mm}^2$ in the middle of the precentral gyrus (Brodmann area 4, [34]) was selected as the ROI (Figure 3). The area belongs to the primary motor cortex. The initial position (IP) was set to C4 electrode point of international 10–20 electroencephalography system so that the ROI was directly beneath the intersection of the FOE coil when the initial rotational angle was 0°. This positioning method is frequently used in clinics [9].

2.6. Local Cortical Quantification.
As the induced E-field distribution depends on local anatomy, we investigated the effects of cortical geometry and complexity on the convergence of the optimization. Two metrics were used in the local cortical measurements: lGI and lFD.

lGI quantifies the amount of cortex buried within the sulcal folds as compared with the amount on the outer visible cortex. A cortex with extensive folding has a large gyrification index, whereas one with limited folding has a small gyrification index. lGI is the ratio of the total pial cortical surface over the perimeter of the brain delineated on 2-D coronal sections. Some neuroimaging processing tools, such as Freesurfer [35], provide pipelines for calculating lGI. However, Freesurfer's automatic pipeline uses the raw T1-weighted MRI as the input. The head models

TABLE 1: Segmented tissues in the human head model.

Tissue	Chinese female	Chinese male	Billie	Duke	Ella	TWU	Japanese male	Japanese female	Norman	Naomi	Korean adult	Korean child	VIP-MAN
Blood	x	x	—	x	—	—	x	x	—	—	x	x	x
Bone	x	x	x	x	x	x	x	x	x	x	x	x	x
Bone marrow	x	x	x	x	x	x	—	—	—	—	—	—	x
Cartilage	x	x	x	x	x	x	—	x	—	—	x	x	—
Cerebellum	x	x	x	—	—	x	x	x	—	—	x	x	x
Dura mater	x	x	—	—	—	—	—	—	—	—	—	—	—
Cerebrospinal fluid	x	x	—	—	—	x	—	—	x	x	x	x	x
Commissura anterior	—	—	x	x	x	—	—	—	—	—	—	—	—
Commissura posterior	—	—	x	x	x	—	—	—	—	—	—	—	—
Connective tissue	—	—	x	x	x	x	—	—	—	—	—	—	—
Eyes	x	x	x	x	x	x	x	x	x	x	x	x	x
Fat	x	x	x	x	x	x	—	—	x	x	x	x	x
Grey matter	x	x	x	x	x	x	x	x	—	x	x	x	x
Hippocampus	x	x	x	x	x	—	—	—	—	—	—	—	—
Hypophysis	x	x	x	x	x	—	—	—	—	—	—	—	—
Hypothalamus	x	x	x	x	x	—	x	x	—	—	—	—	—
Internal air	x	x	x	x	x	—	x	x	—	—	—	—	x
Lymph node	x	x	—	—	—	—	—	—	—	—	—	—	—
Mucosa	—	—	x	x	x	—	—	—	—	—	—	—	—
Muscle	x	x	x	x	x	x	x	x	x	x	x	x	x
Midbrain	—	—	x	x	x	x	—	—	—	—	—	—	—
Nerve	x	x	x	x	x	—	—	—	x	x	x	x	x
Pineal gland	x	x	x	x	x	—	x	x	—	—	—	—	—
Pituitary	—	—	—	—	—	—	x	x	—	—	—	—	—
Pons	—	—	x	x	x	—	—	—	—	—	—	—	—
Salivary gland	x	x	—	—	—	—	—	—	—	—	—	—	—
Skin	x	x	x	x	x	x	x	x	x	x	x	x	—
Teeth	x	x	x	x	x	x	—	—	—	—	—	—	x
Thalamus	—	—	—	—	—	—	—	x	—	—	—	—	x
Tongue	x	x	x	x	x	—	—	x	—	x	x	x	—
White matter	x	x	x	x	x	x	x	x	—	x	x	x	x

used in this study were segmented, and the raw data were unavailable. Therefore, we developed tools to use the segmented models. First, the cortical surface was discretized on an adaptive triangular mesh using Amira (Thermo Fisher Scientific, Waltham, MA). Second, the local gyral vertex was connected on a smoothed surface and subsequently discretized on an adaptive triangular mesh. Accordingly, lGI can be obtained by the division of the two surface areas.

Cortical FD covaries with gyrification [36], and analyses of this relationship are useful for quantifying the convolutional properties of the cortex across multiple scales [37]. There exist several algorithms to calculate the dimensionality measure [38]. We applied a dilation algorithm to measure the 3D structure. Using this method, each voxel of the 3D structure was replaced with a cube of given volume. The cube sizes can be dilated, usually by a multiple of 2, while the number of cubes is changed to fill the 3D volume. After taking the logarithm of both cube size and the count of cubes filled, the FD value was derived as in the following equation:

$$FD_f = -\frac{\Delta \log_2 (\text{count})}{\Delta \log_2 (\text{size})}. \tag{3}$$

The 3D cortical surface under the search surface of the particles was extracted for FD measurement. Calculation of 3D fractal dimensionality was done by a MATLAB program provided by Madan and Kensinger [39].

Both lGI and FD were calculated based on a search surface of $4 \times 4 \, \text{cm}^2$.

3. Results and Discussion

3.1. Efficiency of PSO. Using eight particles, we repeated the optimization of each head model five times. The difference between the five simulations was the initial particle positions, which were randomly generated. The E-field distribution with each optimization is shown in Figure 4. The detailed results are shown in Table 3 and summarized in Table 4. The optimization converged at 4–11 iterations, theoretically corresponding to 192–528 min by serial computing (the actual time cost using the above-mentioned

Table 2: Conductivity, relative permittivity, and density of the tissue.

Tissue	Conductivity (S/m)	Density (g/cm^3)
Blood	$7.00e-1$	1.05
Bone	$2.03e-2$	1.91
Bone marrow	$2.90e-2$	0.98
Cartilage	$1.75e-1$	1.10
Cerebellum	$1.24e-1$	1.05
Dura mater	$5.01e-1$	1.17
Cerebrospinal fluid	2.00	1.01
Commissura anterior	$6.42e-2$	1.04
Commissura posterior	$6.42e-2$	1.04
Connective tissue	$3.85e-1$	1.53
Eyes	2.00	1.00
Fat	$4.23e-2$	0.91
Grey matter	$1.04e-1$	1.04
Hippocampus	$1.04e-1$	1.04
Hypophysis	$5.26e-1$	1.05
Hypothalamus	$5.26e-1$	1.05
Internal air	0	1.00
Lymph node	$5.26e-1$	1.04
Mucosa	$8.25e-4$	1.10
Muscle	$3.31e-1$	1.09
Midbrain	$1.24e-1$	1.04
Nerve	$3.02e-1$	1.07
Pineal gland	$5.26e-1$	1.05
Pituitary	$5.26e-1$	1.05
Pons	$1.24e-1$	1.05
Salivary gland	$3.02e-2$	1.08
Skin	$2.00e-4$	1.11
Teeth	$2.03e-2$	2.18
Thalamus	$1.04e-1$	1.04
Tongue	$2.76e-1$	1.09
White matter	$6.42e-2$	1.04

hardware was approximately 220–560 min). In comparison, the induced E-field strength can be enhanced by up to 116% (Table 3, Korean Adult, #2 optimization), with an overall improvement of about 43% for the 13 head models. The spatial deviation from the IP was up to 18 mm (Table 3).

The maximum shift by optimization was 18 mm: the researchers alternately conducted the brute force simulations (simulations by traversing all possible configurations) on a surface of about 18×18 mm^2 to search for the optimal value, resulting in 3,888 candidate configurations (1 mm resolution and 12 rotational angles for each point). We conducted a validation experiment using a Chinese male head model as an example. The histogram of the calculated maximum E-field strength is shown in Figure 5.

The calculated maximum E-field strength was 2.46 V/m, compared with 2.35 V/m by PSO with less than 70 simulations (8.4 iterations × 8 particles = 64). More than 98% of the simulations were saved, with a difference of only 4%.

Admittedly, the focality of the FOE coil was approximately a few cm^2 [40]. However, using our proposed method, we could manage the E-field distribution in a much finer region. These notions are not contradictory because the present study aimed to direct the peak values to the pre-defined brain regions. In this approach, the operators could reduce the power delivered to the coil so that the above-threshold stimulation was achieved only in the ROI. As such, the coil's performance was exploited to achieve fit with a very narrow stimulation.

The results listed in Tables 3 and 4 were averaged over ROIs of 2×2 mm^2 (i.e., four voxels). Hence, the statistical results for the 99th percentile of E-field strength, which is prescribed by ICNIRP to reduce stair-case errors, are unavailable. The absolute percentage increase may be subject to change when other statistical metrics are applied. As E-field enhancement was found for all of the optimizations, the proposed optimization effectively improved the localized E-field strength. It should be note that the ROI size could potentially affect the performance of the algorithm method. The different ROIs may be used according to the clinical application so that the realistic performance improved need be investigated for various ROI definitions.

The threshold for brain stimulation was above 100 V/m. In the study, we obtained the induced E-field strength at the level of several V/m. There were mainly two reasons for it. Firstly, the coil used in the simulation was about half the diameter of a conventional FOE coil. The advantage was that it had better focality, but with reduced induced E-field strength. To validate our results, we can refer to existing literature using similar coils for rodent stimulation [41]. Secondly, the coil in the study had only one turn. In contrast, the clinical coils usually had 10 to 15 turns. As such, the induced E-field strength was further lowered. However, the purpose of the study was to present an optimization algorithm for the induced E-field strength. The results from this simplified FOE coil were still representative.

3.2. Optimization of PSO Parameters. Previous studies concluded that the best approach to optimize PSO parameters is the rule of thumb, i.e., fixing the inertial weight while carefully selecting c_1 and c_2 [42] or vice versa. In general, parameter selection was empirical. We conducted numerical simulations to investigate parameter selection.

In this study, parametric optimization was initiated in terms of population size. Larger population size can accelerate convergence, but at the cost of an increased number of simulations per iteration. In addition, hardware parallelization should be taken into consideration when deciding the number of particles. Some studies have reported that PSO was not sensitive to population size [27] and that a population size of 20–30 is a conventional choice. We conducted trial simulations using 4, 6, 8, 12, 16, and 20 particles. With 8 particles, a 100% success rate was achieved for all head models. This particle count was selected because it was appropriate for the core size of the current CPU, which facilitated parallelization.

The present study adopted the $c_1 = c_2 = 2.05$. It was proposed by the previous empirical studies on PSO [27]. Some studies have also proposed to fix the sum of c_1 and c_2 to 4.1 while adjusting the ratio of c_1/c_2 from 2.8/1.3 to 1.3/2.8 [43]. We applied these coefficients to our simulations with a step of 0.2, using the Chinese adult female and male head models. The results indicate that there is no significant difference.

(a)   (b)   (c)
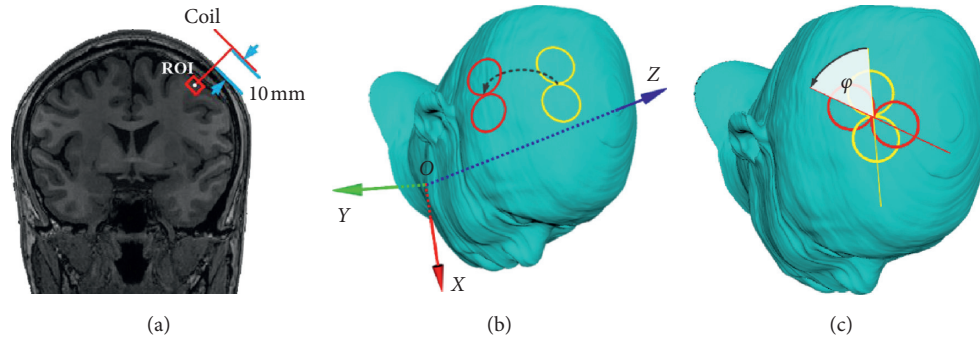
FIGURE 2: Positioning of the coil and the head model. During the stimulation, the distance between the coil and scalp was 10 mm, and its plane was tangential to the surface (a). The coil can move around the surface with a constant separation of 10 mm to the scalp (b). The rotational axis passed through the intersection point of the 8-shape coil and was perpendicular to the coil's surface (c). 0° of the rotational angle was defined when the long axis of the coil was parallel to X coordinate. The rotation angle φ was defined hereafter.
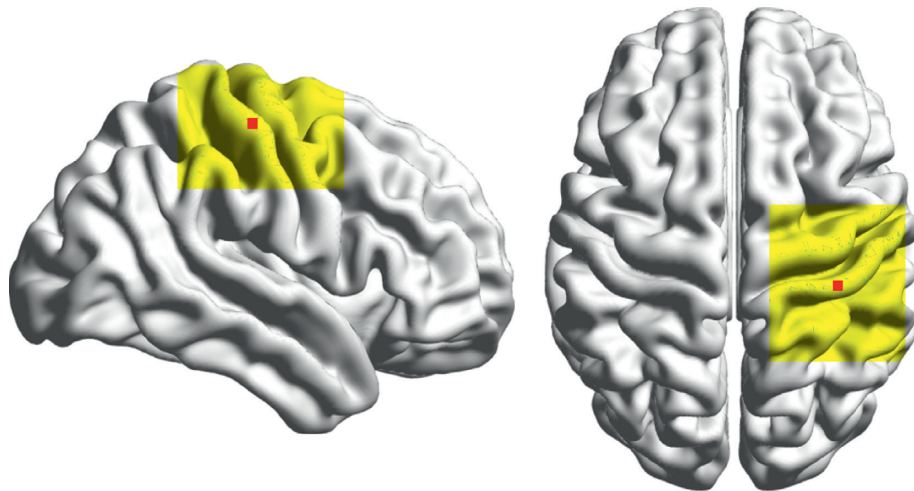

FIGURE 3: ROI (red square) in the numerical simulation for the head model and the searching surface (yellow region).

Prior knowledge could help to further reduce the number of simulations. For example, we may design the initial rotational angles of the FOE so that they are close to perpendicular to the local gyral orientation. It has been reported that this layout could lead to higher E-field strength [9].

Besides PSO, other methods based on brain Atlas [7] and deep neural networks [44] have also shown promise in facilitating accurate brain stimulation.

3.3. Relation between Local Anatomical Complexity and Convergence Rate.
Cortical quantification of the local cortical regions from various head models is shown in Table 5. As the induced E-field distribution was influenced by local anatomy, the convergence rate was assumed to change with the cortical complexity of the local cortex beneath the search surface. We conducted correlational analysis of the results from the 13 head models using Spearman's rank correlation coefficient and estimated the resulting statistical significance ($\alpha = 0.05$). The results were as follows: $r = 0.19$ and $p = 0.53$ for lFD vs. mean E-field strength enhancement, $r = 0.08$ and

$p = 0.81$ for lGI vs. mean E-field strength enhancement, $r = -0.07$ and $p = 0.82$ for lGI vs. mean iteration, and $r = 0.41$, $p = 0.16$ for lGI vs. mean iteration.

The results indicated that there was no significant correlation between local cortical complexity and either the convergence rate or the enhancement to the expected E-field strength. The findings need further investigation using more anatomical head models, which will be performed in our future work.

The measured lGL and FD values fell in the average range for the population, according to anatomical/radiological reports [13, 45]. In addition, the anatomical head models were generated with various segmentation tools and protocols. Accordingly, optimal performance could be expected from a large population.

In addition to anatomical factors, the most effective coil orientation depends on the shape of the induced current pulse. Further, when the first and second phases of the pulse are of similar size, it depends on the intensity of stimulation. Optimal mapping of the human motor cortex with magnetic stimulation requires knowledge of the influences on all these factors [2, 46].
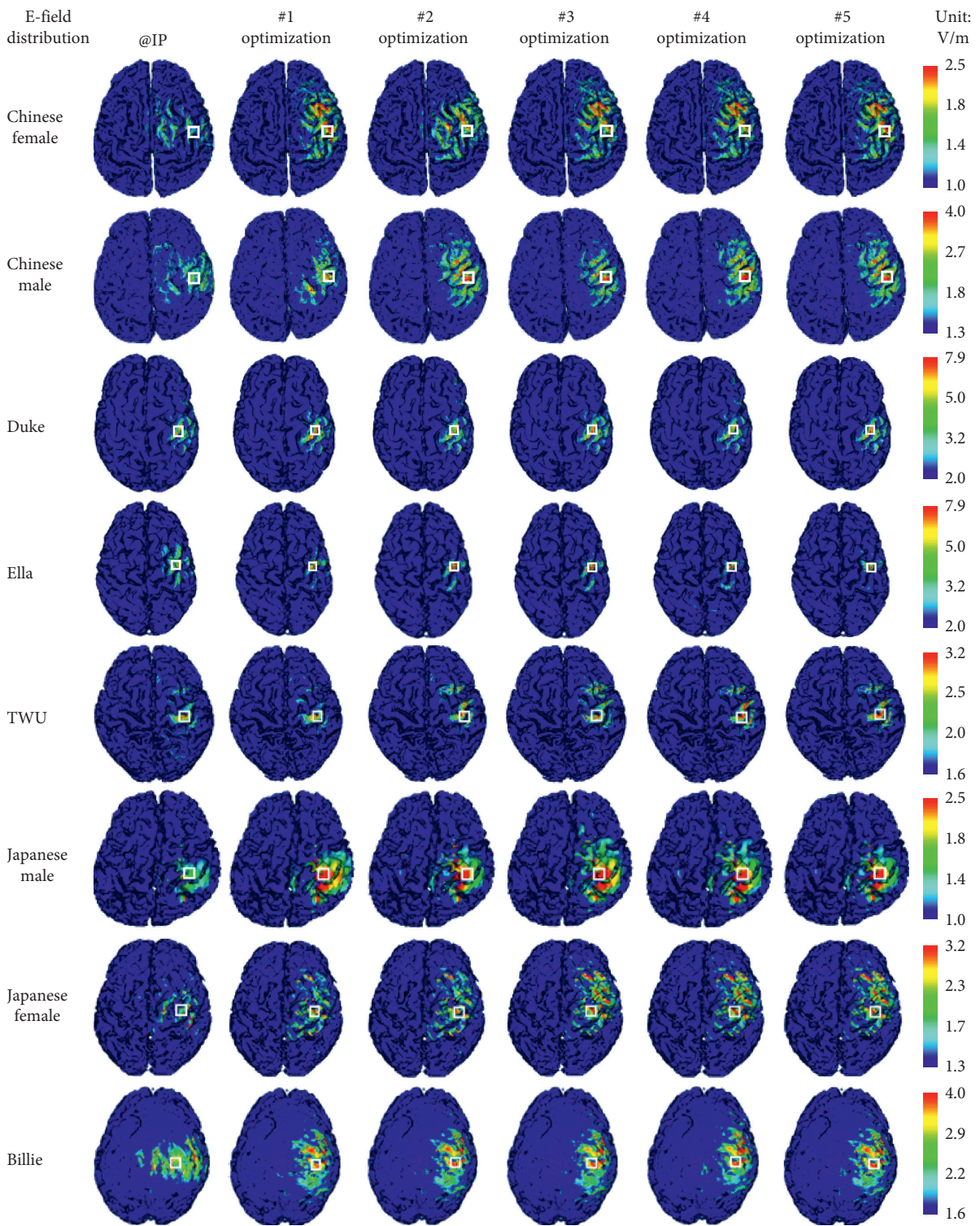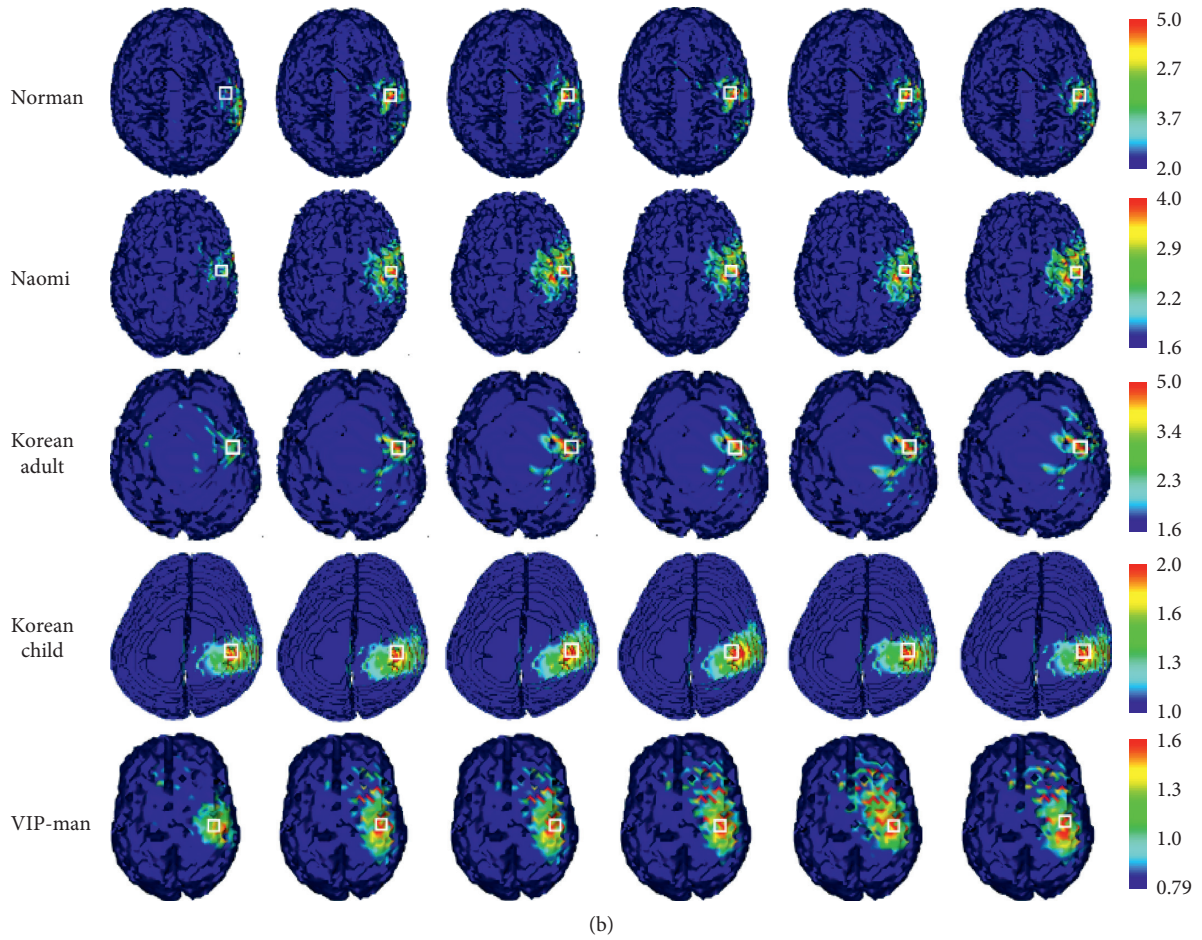
(a)

Figure 4: Continued.

(b)

FIGURE 4: E-field distribution for different head models. ROI is indicated by the square. The results are calculated from the presented configurations. A comparison of the induced E-field strength with the clinical FOE coil can be made by considering the realistic number of coil, the actual current in the coil, and diameters of the coil. The frequency should also be taken into consideration.

TABLE 3: Detailed convergence results for each head model.

Model	Iterations to converge	E-field strength in ROI (IP) in V/m	E-field strength in ROI by optimization (V/m)	E-field strength enhancement (%)	Displacement from IP (mm)	φ (°)
Simulation 1						
Chinese female	10	1.12	1.75	57.62	10.59	48.46
Chinese male	10	1.87	2.39	28.20	14.41	41.81
Billie	7	1.99	3.16	59.28	1.32	87.09
Duke	8	2.76	3.53	27.79	12.83	162.25
Ella	6	2.82	4.32	53.58	5.94	107.71
TWU	6	1.12	1.82	62.86	15.37	32.21
Japanese male	6	1.90	2.50	31.66	7.49	17.73
Japanese female	8	2.30	2.76	20.07	17.03	54.89
Norman	8	2.54	3.89	52.73	13.86	145.69
Naomi	7	1.22	2.01	64.69	2.58	33.23
Korean adult	6	2.10	4.41	109.28	5.68	76.13
Korean child	6	1.56	1.74	11.14	3.11	9.49

TABLE 3: Continued.

Model	Iterations to converge	E-field strength in ROI (IP) in V/m	E-field strength in ROI by optimization (V/m)	E-field strength enhancement (%)	Displacement from IP (mm)	φ (°)
VIP-man	7	1.16	1.64	41.47	4.44	107.48
Simulation 2						
Chinese female	8	1.12	1.76	58.54	5.67	159.82
Chinese male	8	1.87	2.43	30.07	10.16	104.24
Billie	7	1.99	3.12	57.05	4.32	83.41
Duke	8	2.76	3.48	26.31	6.42	165.59
Ella	6	2.82	4.12	46.48	5.69	86.66
TWU	6	1.12	1.92	71.32	12.09	88.49
Japanese male	6	1.90	2.51	32.40	18.22	61.17
Japanese female	6	2.30	2.73	18.85	8.54	26.35
Norman	8	2.54	3.84	50.90	16.12	158.84
Naomi	8	1.22	2.04	67.09	9.49	34.04
Korean adult	7	2.10	4.56	116.57	5.27	69.35
Korean child	7	1.56	1.77	13.24	3.25	18.91
VIP-man	7	1.16	1.67	44.47	3.91	119.99
Simulation 3						
Chinese female	9	1.12	1.75	57.19	16.80	77.73
Chinese male	10	1.87	2.43	30.33	5.47	98.17
Billie	8	1.99	3.13	57.88	4.86	78.56
Duke	7	2.76	3.51	27.39	9.79	178.76
Ella	5	2.82	4.11	46.04	10.05	109.07
TWU	6	1.12	2.01	79.22	16.09	172.07
Japanese male	7	1.90	2.50	31.87	5.49	14.65
Japanese female	9	2.30	2.87	25.00	8.65	62.05
Norman	7	2.54	3.82	49.99	17.01	147.85
Naomi	7	1.22	1.99	63.13	1.66	30.42
Korean adult	7	2.10	4.52	114.92	4.33	67.99
Korean child	7	1.56	1.79	14.51	3.40	19.36
VIP-man	8	1.16	1.66	43.24	6.67	65.01
Simulation 4						
Chinese female	10	1.12	1.76	58.60	7.31	0.26
Chinese male	8	1.87	2.49	33.25	14.44	118.79
Billie	6	1.99	3.12	57.30	14.83	82.37
Duke	8	2.76	3.40	23.29	13.01	176.63
Ella	9	2.82	4.13	46.65	13.51	78.73
TWU	6	1.12	1.83	63.96	14.14	25.58
Japanese male	5	1.90	2.48	30.89	9.94	38.74
Japanese female	8	2.30	2.71	17.89	3.44	51.97
Norman	8	2.54	3.79	48.93	13.39	138.17
Naomi	9	1.22	1.91	56.97	8.11	34.79
Korean adult	8	2.10	4.51	114.13	7.22	71.33

TABLE 3: Continued.

Model	Iterations to converge	E-field strength in ROI (IP) in V/m	E-field strength in ROI by optimization (V/m)	E-field strength enhancement (%)	Displacement from IP (mm)	φ (°)
Korean child	6	1.56	1.73	10.98	1.93	1.71
VIP-man	6	1.16	1.69	45.97	17.64	122.74
Simulation 5						
Chinese female	11	1.12	1.77	59.08	8.85	93.97
Chinese male	6	1.87	2.44	31.00	14.88	117.89
Billie	4	1.99	3.20	61.11	4.43	81.44
Duke	9	2.76	3.34	21.29	7.62	163.16
Ella	4	2.82	4.24	50.74	8.82	79.7
TWU	9	1.12	1.93	72.46	11.18	18.37
Japanese male	11	1.90	2.48	30.49	15.94	25.12
Japanese female	7	2.30	2.78	20.79	13.00	61.98
Norman	7	2.54	3.80	49.39	12.40	157.69
Naomi	7	1.22	2.01	65.20	10.56	33.21
Korean adult	7	2.10	4.54	115.76	3.96	69.43
Korean child	6	1.56	1.74	11.65	1.84	1.02
VIP-man	8	1.16	1.67	44.32	8.53	118.83

The values were calculated with the incident current to the coil as 1 kA at 2.24 kHz.

TABLE 4: Statistical results based on 5 times of optimization.

	Iterations	E-field strength enhancement compared with IP (%)	Displacement from IP (mm)	φ (°)
Chinese female	9.60 ± 0.94	58.18 ± 0.63	9.84 ± 3.84	76.05 ± 52.62
Chinese male	8.40 ± 1.88	30.57 ± 1.49	11.87 ± 3.63	96.18 ± 28.31
Billie	6.40 ± 1.25	58.52 ± 1.38	5.95 ± 4.61	82.57 ± 2.77
Duke	8.00 ± 0.92	25.21 ± 2.30	9.94 ± 2.66	169.28 ± 6.99
Ella	6.00 ± 1.85	48.69 ± 2.71	8.80 ± 2.88	92.37 ± 13.36
TWU	6.60 ± 2.89	69.96 ± 5.48	13.77 ± 1.87	67.34 ± 57.95
Japanese male	7.00 ± 2.53	31.47 ± 0.63	11.42 ± 4.88	31.48 ± 17.01
Japanese female	7.60 ± 1.33	21.32 ± 2.16	10.13 ± 4.58	51.45 ± 13.16
Norman	7.60 ± 0.49	50.39 ± 1.34	14.56 ± 1.73	149.65 ± 7.74
Naomi	7.60 ± 0.80	63.42 ± 3.46	6.48 ± 3.66	33.14 ± 1.48
Korean adult	7.00 ± 0.63	114.13 ± 2.56	5.29 ± 1.15	70.85 ± 2.85
Korean child	6.40 ± 0.49	12.30 ± 1.36	2.71 ± 0.68	10.10 ± 7.96
VIP-man	7.20 ± 0.75	43.89 ± 1.49	8.24 ± 4.98	106.81 ± 21.54

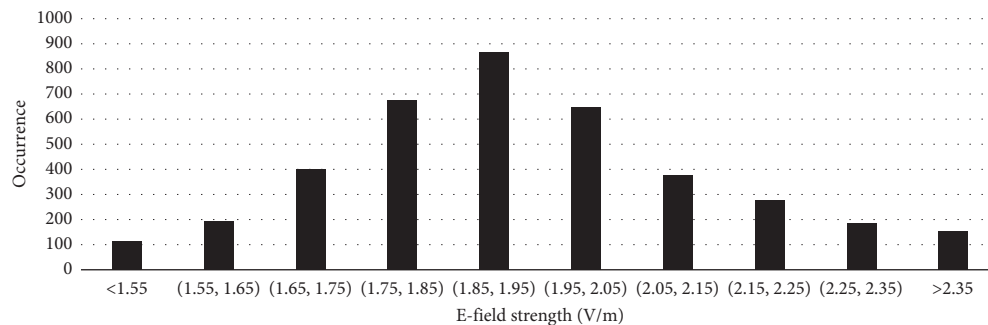The values are presented as mean ± standard deviation.

FIGURE 5: The histogram of the calculated maximum E-field strength. The results are calculated from the presented configurations. A comparison of the induced E-field strength with the clinical FOE coil can be made by considering the realistic number of coil, the actual current in the coil, and the diameters of the coil. The frequency should also be taken into consideration.

TABLE 5: Local geometric feature for the head model at the searching cortex.

Model	FD	lGI
Chinese female	2.23	3.52
Chinese male	2.38	2.85
Billie	2.42	2.50
Duke	2.21	1.83
Ella	2.33	2.02
TWU	2.45	3.46
Japanese male	1.97	2.59
Japanese female	2.02	2.75
Norman	2.19	1.84
Naomi	2.20	2.22
Korean adult	2.09	1.69
Korean child	2.12	1.41
VIP-man	2.01	1.37

4. Conclusion

This study proposed numerical methods to optimize TMS coil positioning according to clinical needs. The application of PSO-based optimization to TMS coil positioning was first studied in this work. The versatility and efficiency of the optimizer have been numerically demonstrated. This study confirmed that the proposed algorithm is valid and efficient for providing optimal plans (in terms of induced E-field strength in the ROI) within a clinically acceptable period. A FOE coil was used in this study, and the proposed method further exploited its performance in brain stimulation. In conclusion, PSO can enhance the E-field strength in an ROI by a mean value of about 48%. The derived parameters can benefit robotic neuroimaging navigation systems by facilitating stable and desired cortical activation.

Data Availability

The data used to support the findings of this study are available from the corresponding author upon request.

Conflicts of Interest

The authors report no conflicts of interest in this work. None of the authors have any personal or financial involvement with organizations that have a financial interest in its content.

Authors' Contributions

Congsheng Li and Chang Liu contributed equally to this work.

Acknowledgments

References

[1] M. Hallett, "Transcranial magnetic stimulation and the human brain," *Nature*, vol. 406, no. 4792, pp. 147–150, 2000.

[2] A. Opitz, M. Windhoff, R. M. Heidemann, R. Turner, and A. Thielscher, "How the brain tissue shapes the electric field induced by transcranial magnetic stimulation," *Neuroimage*, vol. 58, no. 3, pp. 849–859, 2011.

[3] A. M. Janssen, S. M. Rampersad, F. Lucka et al., "The influence of sulcus width on simulated electric fields induced by transcranial magnetic stimulation," *Physics in Medicine and Biology*, vol. 58, no. 14, pp. 4881–4896, 2013.

[4] A. Thielscher, A. Opitz, and M. Windhoff, "Impact of the gyral geometry on the electric field induced by transcranial magnetic stimulation," *Neuroimage*, vol. 54, no. 1, pp. 234–243, 2011.

[5] I. Laakso, A. Hirata, and Y. Ugawa, "Effects of coil orientation on the electric field induced by TMS over the hand motor area," *Physics in Medicine and Biology*, vol. 59, no. 1, pp. 203–218, 2014.

[6] L. Richter, G. Neumann, S. Oung et al., "Optimal coil orientation for transcranial magnetic stimulation," *PLoS One*, vol. 8, no. 4, Article ID e60358, 2013.

[7] J. Gomez-Tames, A. Hamasaka, I. Laakso, A. Hirata, and Y. Ugawa, "Atlas of optimal coil orientation and position for TMS: a computational study," *Brain Stimulation*, vol. 11, no. 4, pp. 839–848, 2018.

[8] A. Janssen, T. Oostendorp, and D. Stegeman, "The coil orientation dependency of the electric field induced by TMS for M1 and other brain areas," *Journal of Neuroengineering & Rehabilitation*, vol. 12, no. 1, pp. 1–13, 2015.

[9] S. Rossi, M. Hallett, P. M. Rossini, and A. Pascual-Leone, "Safety, ethical considerations, and application guidelines for the use of transcranial magnetic stimulation in clinical practice and research," *Clinical Neurophysiology*, vol. 120, no. 12, pp. 2008–2039, 2009.

[10] A. S. Ferguson, D. Durand, and T. Dalbasti, "Optimization of coil design for neuronal excitation by magnetic stimulation," in *Proceedings of the IEEE International Conference of the Engineering*, pp. 1254-1255, Philadelphia, PA, USA, November 1989.

[11] J. Liu, J. Lu, C. Liu, and Y. Hu, "Coil arrays modeling and optimization for transcranial magnetic stimulation," in *Proceedings of the IEEE International Conference on Biomedical Engineering & Informatics*, pp. 1–5, Tianjin, China, October 2009.

[12] H. Xiong, J. H. Shi, X.-W. Hu, and J.-Z. Li, "The focusing optimization of transcranial magnetic stimulation system," *Progress in Electromagnetics Research M*, vol. 48, pp. 145–154, 2016.

[13] M. Schaer, M. B. Cuadra, L. Tamarit, F. Lazeyras, S. Eliez, and J.-P. Thiran, "A surface-based approach to quantify local cortical gyrification," *IEEE Transactions on Medical Imaging*, vol. 27, no. 2, pp. 161–170, 2008.

[14] C. R. Madan and E. A. Kensinger, "Cortical complexity as a measure of age-related brain atrophy," *Neuroimage*, vol. 134, pp. 617–629, 2006.

[15] T. Wu, L. Tan, Q. Shao et al., "Chinese adult anatomical models and the application in evaluation of RF exposures," *Physics in Medicine and Biology*, vol. 56, no. 7, pp. 2075–2089, 2011.

[16] T. Wu, L. Tan, Q. Shao et al., "Slice-based supine to standing posture deformation for Chinese anatomical models and the dosimetric results by wide band frequency electromagnetic

field exposure: morphing," *Radiation Protection Dosimetry*, vol. 142, no. 16, pp. 26–30, 2012.

[17] A. Christ, W. Kainz, E. G. Hahn et al., ""The virtual family—development of surface-based anatomical models of two adults and two children for dosimetric simulations," *Physics in Medicine and Biology*, vol. 55, no. 2, pp. 23–38, 2010.

[18] T. Wu, Q. Shao, and L. Yang, "Simplified segmented human models for whole body and localised SAR evaluation of 20 MHz to 6 GHz electromagnetic field exposures," *Radiation Protection Dosimetry*, vol. 153, no. 3, pp. 266–272, 2012.

[19] T. Nagaoka, S. Watanabe, K. Sakurai et al., "Development of realistic high-resolution whole-body voxel models of Japanese adult males and females of average height and weight, and application of models to radio-frequency electromagnetic-field dosimetry," *Physics in Medicine and Biology*, vol. 49, no. 1, pp. 1–15, 2003.

[20] D. G. Jones, "A realistic anthrompomorphic phantom for calculating specific absorbed fractions of energy deposited from internal gamma emitters," *Radiation Protection Dosimetry*, vol. 79, no. 1, pp. 411–414, 1998.

[21] P. Dimbylow, "Development of the female voxel phantom, NAOMI, and its application to calculations of induced current densities and electric fields from applied low frequency magnetic and electric fields," *Physics in Medicine and Biology*, vol. 50, no. 6, pp. 1047–1070, 2005.

[22] A.-K. Lee, W. Y. Choi, M. S. Chung, H.-D. Choi, and J.-I. Choi, "Development of Korean male body model for computational dosimetry," *ETRI Journal*, vol. 28, no. 1, pp. 107–110, 2006.

[23] A.-K. Lee, J.-K. Byun, J. S. Park, H.-D. Choi, and J. Yun, "Development of 7-year-old Korean child model for computational dosimetry," *ETRI Journal*, vol. 31, no. 2, pp. 237–239, 2009.

[24] M. J. Ackerman, V. M. Spitzer, A. L. Scherzinger, and D. G. Whitlock, "The visible human dataset: an image resource for anatomical visualization," *Medinfo*, vol. 8, no. Pt 2, pp. 1195–1198, 2005.

[25] S. Gabriel, R. W. Lau, and C. Gabriel, "The dielectric properties of biological tissues: II. Measurements in the frequency range 10 Hz to 20 GHz," *Physics in Medicine and Biology*, vol. 41, no. 11, pp. 2251–2269, 1996.

[26] S. Gabriel, R. W. Lau, and C. Gabriel, "The dielectric properties of biological tissues: III. Parametric models for the dielectric spectrum of tissues," *Physics in Medicine and Biology*, vol. 41, no. 11, pp. 2271–2293, 1996.

[27] Y. Shi and R. C. Eberhart, "Empirical study of particle swarm optimization," in *Proceedings of the IEEE International Congress on Evolutionary Computation*, vol. 3, pp. 1945–1950, Honolulu, HI, USA, May 2002.

[28] Y. Shi and R. Eberhart, "A modified particle swarm optimizer," in *Proceedings of the IEEE International Conference on Evolutionary Computation*, pp. 69–73, Anchorage, AK, USA, May 1998.

[29] C. Li, Z. Ye, Y. Wei, and T. Wu, "An optimized block forward-elimination and backward-substitution algorithm for GPU accelerated ILU preconditioner in evaluating the induced electric field during transcranial magnetic stimulation," *Bioelectromagnetics*, vol. 40, no. 4, pp. 278–284, 2019.

[30] A. Pascual-Leone and V. Walsh, "Transcranial magnetic stimulation," *Brain Mapping: The Methods*, vol. 2, no. 4, pp. 255–290, 2002.

[31] R. Möttönen, J. Rogers, and K. E. Watkins, "Stimulating the lip motor cortex with transcranial magnetic stimulation," *Journal of Visualized Experiments*, vol. 88, pp. 1–7, 2014.

[32] T. C. Harrison, O. G. S. Ayling, and T. H. Murphy, "Distinct cortical circuit mechanisms for complex forelimb movement and motor map topography," *Neuron*, vol. 74, no. 2, pp. 397–409, 2012.

[33] G. W. Thickbroom, B. A. Phillips, I. Morris, M. L. Byrnes, and F. L. Mastaglia, "Isometric force-related activity in sensorimotor cortex measured with functional MRI," *Experimental Brain Research*, vol. 121, no. 1, pp. 59–64, 1998.

[34] L. J. Garey, *Brodmann's "Localisation in the Cerebral Cortex"*, Imperial College, London, UK, 2000.

[35] B. Fischl, "FreeSurfer," *NeuroImage*, vol. 62, no. 2, pp. 774–781, 2012.

[36] R. D. King, B. Brown, M. Hwang, T. Jeon, and A. T. George, "Fractal dimension analysis of the cortical ribbon in mild alzheimer's disease," *Neuroimage*, vol. 53, no. 2, pp. 471–479, 2010.

[37] S. L. Free, S. M. Sisodiya, M. J. Cook, D. R. Fish, and S. D. Shorvon, "Three-dimensional fractal analysis of the white matter surface from magnetic resonance images of the human brain," *Cerebral Cortex*, vol. 6, no. 6, pp. 830–836, 1996.

[38] E. Fernández and H. F. Jelinek, "Use of fractal theory in neuroscience: methods, advantages, and potential problems," *Methods*, vol. 24, no. 4, pp. 309–321, 2001.

[39] C. R. Madan and E. A. Kensinger, "Age-related differences in the structural complexity of subcortical and ventricular structures," *Neurobiology of Aging*, vol. 50, pp. 87–95, 2017.

[40] Z.-D. Deng, S. H. Lisanby, and A. V. Peterchev, "Electric field depth-focality tradeoff in transcranial magnetic stimulation: simulation comparison of 50 coil designs," *Brain Stimulation*, vol. 6, no. 1, pp. 1–13, 2013.

[41] L. J. Crowther, R. L. Hadimani, A. G. Kanthasamy, and D. C. Jiles, "Transcranial magnetic stimulation of mouse brain using high-resolution anatomical models," *Journal of Applied Physics*, vol. 115, no. 17, p. 17B303, 2014.

[42] R. C. Eberhart, "Comparing inertia weights and constriction factors in particle swarm optimization," in *Proceedings of the IEEE International Congress on Evolutionary Computation*, pp. 84–88, La Jolla, CA, USA, July 2000.

[43] A. Carlisle and G. Dozier, "An off-the-shelf PSO," in *Proceedings of the Workshop on Particle Swarm Optimization*, vol. 1, pp. 1–6, Indianapolis, IN, USA, April 2001.

[44] T. Yokota, T. Maki, T. Nagata et al., "Real-time estimation of electric fields induced by transcranial magnetic stimulation with deep neural networks," *Brain Stimulation*, 2019, In press.

[45] L. Zhang and G. H. Yue, "Fractal dimension studies of the brain shape in aging and neurodegenerative diseases," *The Fractal Geometry of the Brain, Springer Series in Computational Neuroscience*, pp. 213–232, Springer, New York, NY, USA, 2016.

[46] B. Roth and M. Hallett, "Optimal focal transcranial magnetic activation of the human motor cortex: effects of coil orientation, shape," *Journal of Clinical Neurophysiology*, vol. 9, no. 1, pp. 132–136, 1992.